THE ASTROPHYSICAL JOURNAL, 593:258–271, 2003 August 10

CONSTRAINTS ON A UNIVERSAL STELLAR INITIAL MASS FUNCTION FROM ULTRAVIOLET TO NEAR-INFRARED GALAXY LUMINOSITY DENSITIES

IVAN K. BALDRY AND KARL GLAZEBROOK
Department of Physics and Astronomy, Johns Hopkins University, Baltimore, MD 21218-2686
Received 2003 February 21; accepted 2003 April 23

ABSTRACT

We obtain constraints on the slope of a universal stellar initial mass function (IMF) over a range of model cosmic star formation histories (SFHs) using $z \approx 0.1$ luminosity densities in the range from 0.2 to 2.2 μm. The age-IMF degeneracy of the integrated spectra of stellar populations can be broken for the universe as a whole by using direct measurements of (relative) cosmic SFH from high-redshift observations. These have only marginal dependence on uncertainties in the IMF, whereas fitting to local luminosity densities depends strongly on both cosmic SFH and the IMF. We fit to these measurements using population synthesis and find the best-fit IMF power-law slope to be $\Gamma = 1.15 \pm 0.2$ (assuming $dN/d\log m \propto m^{-\Gamma}$ for 0.5–120 $M_\odot$ and $m^{-0.5}$ for 0.1–0.5 $M_\odot$). This $M > 0.5\ M_\odot$ slope is in good agreement with the Salpeter IMF slope ($\Gamma = 1.35$). A strong upper limit of $\Gamma < 1.7$ is obtained, which effectively rules out the Scalo IMF because its fraction of high-mass stars is too low. This upper limit is at the 99.7% confidence level if we assume a closed-box chemical evolution scenario and 95% if we assume constant solar metallicity. Fitting to the Hα line luminosity density, we obtain a best-fit IMF slope in good agreement with that derived from broadband measurements. Marginalizing over cosmic SFH and IMF slope, we obtain (95% confidence ranges) $\Omega_{\rm stars} = (1.1\text{–}2.0) \times 10^{-3}\ h^{-1}$ for the stellar mass density, $\rho_{\rm SFR} = (0.7\text{–}4.1) \times 10^{-2}\ h\ M_\odot\ {\rm yr}^{-1}\ {\rm Mpc}^{-3}$ for the star formation rate density, and $\rho_L = (1.2\text{–}1.7) \times 10^{35}\ h$ W Mpc^{-3} for the bolometric, attenuated, stellar luminosity density (0.09–5 μm). Comparing this total stellar emission with an estimate of the total dust emission implies a relatively modest average attenuation in the UV ($\lesssim 1$ mag at 0.2 μm).

Subject headings: galaxies: evolution — stars: luminosity function, mass function — ultraviolet: galaxies

1. INTRODUCTION

The luminosity density of the universe in the range from about 0.2 to 2.2 μm, mid-UV to near-IR, is dominated by stellar emission. This wavelength range spans the peak in the spectra (f_ν) of stars with effective temperatures from about 20,000 down to 2000 K. Therefore, measurements of the luminosity density in various broadbands across this range provide a powerful constraint on cosmic star formation history (SFH) and/or a universal stellar initial mass function (IMF).

The stellar IMF describes the relative probability of stars of different masses forming (see Gilmore & Howell 1998 for recent reviews and analyses). Its importance crosses many fields of astronomy, from, for example, star formation (testing theoretical models) to cosmic chemical evolution (heavy-metal production from high-mass stars). It is widely used in the study of the SFH of galaxies from their integrated spectra. Generally, an IMF is assumed and used as an input to evolutionary stellar population synthesis models, and these models are fitted to integrated spectra.

The first calculation of an IMF was made by Salpeter (1955) on the basis of the observed luminosity function of solar neighborhood stars, converting to mass, correcting for main-sequence lifetimes, and assuming that the star formation rate (SFR) has been constant for the last 5 Gyr. Despite the uncertainties in mass-to-light ratios, stellar lifetimes, and the SFR, this result (a power-law slope of -1.35 measured from about 0.3–15 $M_\odot$) is still commonly used today.[1]

Measurements of the solar neighborhood IMF were reviewed by Scalo (1986), producing an IMF with a mass fraction peak around 0.5–1 $M_\odot$ (Fig. 1). When applied to galaxy populations, this IMF is unable to reproduce Hα luminosities (Kennicutt, Tamblyn, & Congdon 1994), and when applied to cosmic evolution, it is unable to match observed mean galaxy colors (Madau, Pozzetti, & Dickinson 1998) because its fraction of high-mass stars ($M > 10\ M_\odot$) is too low.

In a more recent review by Scalo (1998), he concluded that the field star IMF was of questionable use for a number of reasons (e.g., the derived IMF in the range 0.9–1.4 $M_\odot$ depends strongly on the assumed solar neighborhood SFH). Instead, he summarized the results from studying star clusters in a triple-index power-law IMF as an estimate of an average IMF (Fig. 1). He also noted that "if the existing empirical estimates of the IMF are taken at face value, they present strong evidence for variations, and these variations do not seem to depend systematically on physical variables such as metallicity or stellar density." The observed IMF variations from stellar counts could be largely due to statistical fluctuations and/or observational biases such as mass segregation within a star cluster (Elmegreen 1999). These points, if correct, mean that the concept of a universal IMF is highly useful in the study of integrated spectra of galaxies (since they are mostly the result of many star formation regions and episodes), but the IMF is still uncertain at the level of 0.5 in the power-law slopes. By "universal IMF," we mean an IMF that represents the average in a significant majority of galaxies and over a significant majority of cosmic time.

Measurements of the cosmic luminosity densities represent the $\lambda/\Delta\lambda \sim 6$ components of the "cosmic spectrum,"

[1] The Salpeter IMF power-law slope is -1.35 with respect to logarithmic mass bins and -2.35 with respect to linear mass bins.

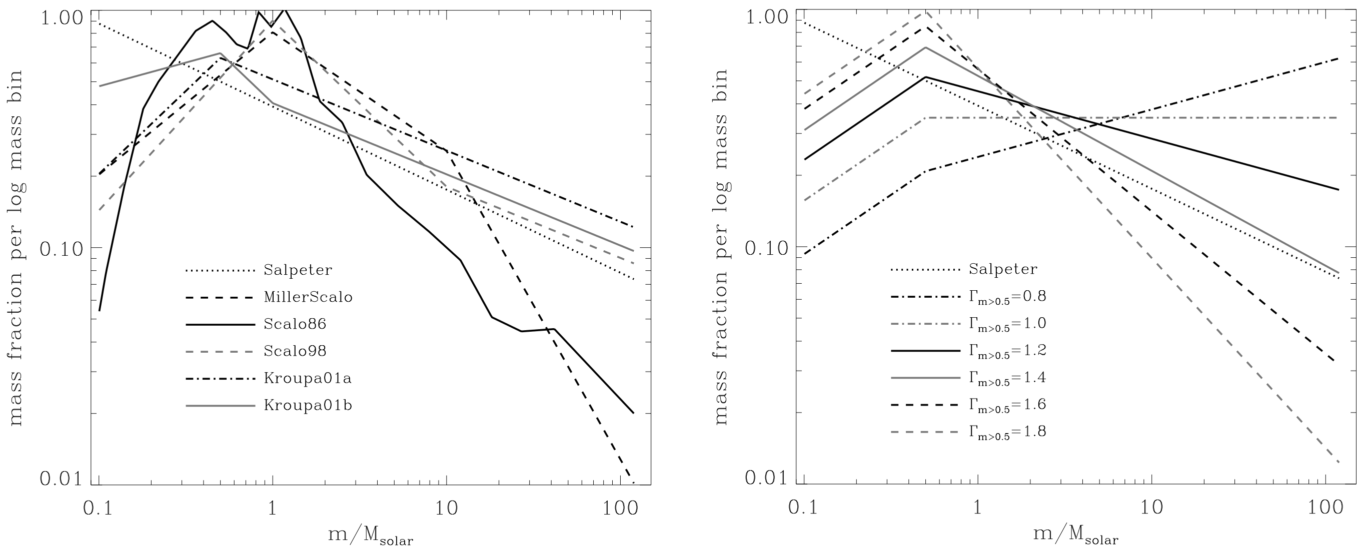

FIG. 1.—Stellar initial mass functions: mass fraction (per logarithmic mass bin) vs. mass for the Salpeter (1955) IMF, the Miller & Scalo (1979) IMF, the Scalo (1986, 1998) IMFs, the Kroupa (2001) IMFs (*left-hand panel*), and the IMF parameterization of eq. (3) (*right-hand panel*). All are assumed to be valid over the range 0.1–120 $M_\odot$. The integral of each curve is set to unity. Note that the slopes of the lines are equivalent to $1 - \Gamma$ [$= d\log(mn_{\log m})/d\log(m)$; see eq. (3) for definitions]. The Γ values for $M > 1\ M_\odot$ for the published IMFs are 1.35 (Salpeter 1955), 1.5/2.3 (Miller & Scalo 1979), $\sim$2.05/1.5 (Scalo 1986), 1.7/1.3 (Scalo 1998), and 1.3 (Kroupa 2001) (see also Table 2).

which is the luminosity-weighted, average galaxy spectrum (Baldry et al. 2002). Thus, if there is a universal IMF, it should certainly apply to this spectrum, and constraints on the IMF can be obtained by fitting population synthesis models. These constraints are degenerate with the assumed cosmic SFH. However, cosmic SFH is generally more accurately quantified than the SFH of any individual galaxy other than in the Local Group. For example, star-forming galaxies have been observed as far back as $z \sim 5$ (Dey et al. 1998), and there is evidence for reionization as early as $z \sim 20$ (Kogut et al. 2003), which for a universe age of 13.7 ± 0.2 Gyr (Spergel et al. 2003) gives a time of 12.3–13.7 Gyr since the onset of a significant rate of star formation in the universe. The results for individual galaxies are often limited by age-metallicity degeneracy (Worthey 1994) and recent bursts of star formation, which can disguise their underlying age (Barbaro & Poggianti 1997). Given our knowledge of cosmic SFH, we can then place constraints on a universal IMF by limiting the SFH we consider.

The primary knowledge of cosmic SFH comes from measuring the comoving density of SFR indicators at various redshifts (Madau et al. 1996). These SFR indicators include UV luminosities and emission-line luminosities that are dominated by light from short-lived high-mass stars. The conversion to SFR depends on the IMF. However, the *relative* cosmic SFH is well defined if the same indicator is used at each redshift regardless of the assumed IMF. Even if the indicator varies (e.g., 0.2–0.3 μm rest-frame UV), the derived cosmic SFH is less sensitive to the slope of the IMF than the local luminosity densities (0.2–2.2 μm). It is this principle that enables constraints on a universal IMF.

An analysis of this type was applied by Madau et al. (1998) using various luminosity densities (0.15–2.2 μm) spread over a range of redshifts (0–4). They fitted cosmic SFHs for three different IMFs. Here we use a more quantitative approach to constrain a universal IMF slope and use more accurate, recent, local ($z \approx 0.1$) luminosity density measurements. Note that we assume that there is a universal IMF and do not constrain any variation in the IMF between different galaxies (see, e.g., Wyse 1997 and Kroupa 2002 for evidence for an invariant IMF). Even if there is some variation, the results presented here could be regarded as constraints on a luminosity-weighted, average IMF.

To summarize, if the cosmic SFH is assumed to be known, on the basis of measurements of various SFR indicators with redshift, then local luminosity density measurements provide a constraint on a universal stellar IMF. The other principal factors to consider are chemical evolution (metallicity) and dust attenuation.

The plan of the paper is as follows. In § 2 we describe details of recent luminosity density measurements. The measurements are illustrated in Figure 2 and summarized in Table 1. In § 3 we describe our modeling and fitting procedures. A summary of the parameters used in the modeling is given in § 3.5. In §§ 4 and 5 we present our results and conclusions.

2. LUMINOSITY DENSITY MEASUREMENTS

In this section we summarize the details of various luminosity density measurements and their conversion to AB magnitudes (Oke & Gunn 1983) per comoving Mpc^3. The zero point of the AB *absolute* magnitude scale is 4.345×10^{13} W Hz^{-1} (3631 Jy for *apparent* magnitudes). In general, an estimate of the total luminosity density from the galaxy population is obtained by an analytical integration of the Schechter (1976) function parameters given by

$$j = M_* - 2.5\log\left[\phi_*\Gamma_f(\alpha + 2)\right] + \mathscr{C}\ , \tag{1}$$

where Γ_f is the gamma function and $\mathscr{C}$ represents corrections from the magnitude system defining the luminosity function to total AB magnitudes. The final luminosity densities are quoted for a cosmology where $(h, \Omega_{m_0}, \Omega_{\Lambda_0}) = (1.0,\ 0.3,\ 0.7)$ and $h = H_0/100$ km s^{-1} Mpc^{-1}. The surveys select redshifts to a limiting magnitude in the same wavelength as that of the luminosity density measurement.

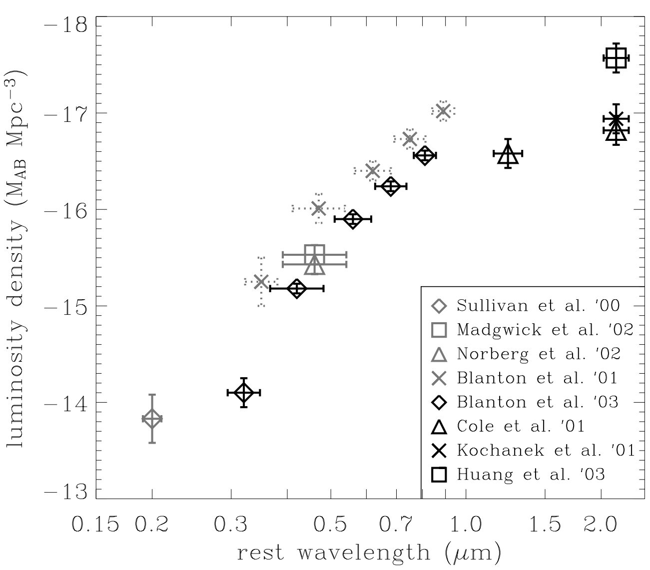

FIG. 2.—Local luminosity densities: absolute AB magnitudes per Mpc^3 $[(h, \Omega_{m_0}, \Omega_{\Lambda_0}) = (1.0,\ 0.3,\ 0.7)]$ vs. wavelength. The vertical bars represent uncertainties, while the horizontal bars represent FWHM of the bandpasses. See Table 1 and § 2 for details. We use the Sullivan et al. (2000), Blanton et al. (2003b), and *J*- and *K*-band results for our fitting.

2.1. *Ultraviolet:* 0.2 μm

An analysis of a mid-UV selected redshift survey is presented by Sullivan et al. (2000). The imaging for this survey covers about 6 deg^2 to a depth of about 21 AB magnitudes using the FOCA balloon-borne telescope (Milliard et al. 1992). The filter response approximates a Gaussian centered at 2015 Å with FWHM of 188 Å. The survey area covers four fields chosen with very low Milky Way (MW) extinction $[E(B-V) \leq 0.015]$. Follow up spectroscopy was obtained using multiobject, optical spectrographs on the WIYN and William Herschel Telescopes (Treyer et al. 1998).

Sullivan et al. measured the local luminosity density using a sample of about 200 galaxies ($0 < z < 0.4$) to estimate the luminosity function. The Schechter parameters without dust-correction were

$$(M_*, \phi_*, \alpha) = (-20.59,\ 0.00955,\ -1.51)\ .$$

Integrating this function gives −16.18, and converting to AB magnitudes gives −13.93 using $m_{\rm AB} = m_{2000} + 2.25$ (Milliard et al. 1992). We also correct the measurement to our default world model of $(\Omega_{m_0}, \Omega_{\Lambda_0}) = (0.3,\ 0.7)$ from (1.0, 0.0) assuming a redshift of 0.15. This gives a correction of about +0.1 mag. The formal uncertainty from the fitting is 0.13 mag. However, there are additional uncertainties: absolute calibration (<0.25 mag), MW extinction (<0.15 mag), conversion to total magnitudes (<0.1 mag), large-scale structure, incompleteness corrections, and so on. We will assume an additional 1 σ uncertainty of 0.2 to be added in quadrature, so that $j = -13.83 \pm 0.25$.

The limit of this survey is $m_{2000} = 18.5$, which corresponds to M_* galaxies at $z \approx 0.2$. With a steep faint-end slope of −1.5, the luminosity-weighted mean redshift is around 0.15, corresponding to the redshift position plotted by Sullivan et al. This is higher than our fiducial redshift of 0.10 (see below), giving a higher luminosity for any declining cosmic SFR at $z < 0.5$. However, this may be counteracted by the lack of MW-extinction and total-magnitude corrections. For simplicity and since we do not want to assume a cosmic SFH and IMF, we will use the luminosity density as it was measured. Note that a couple of galaxies with obvious active galactic nucleus (AGN) characteristics were removed from their sample. We will assume that the measured luminosity density does not have a strong, non-stellar, AGN component. Neither Sullivan et al. (2000) nor Contini et al. (2002) found strong evidence for significant AGN contamination on the basis of emission-line flux ratios.

2.2. *Optical:* 0.3–0.9 μm

The Sloan Digital Sky Survey (SDSS) (York et al. 2000; Stoughton et al. 2002) has imaged over 2000 deg^2 in five bandpasses (*ugriz*) with effective wavelengths from 0.35 to 0.9 μm to a depth of about 21–22 AB magnitudes. Follow-

TABLE 1

LOCAL LUMINOSITY DENSITIES FROM VARIOUS SURVEYS ($0 < \bar{z} < 0.2$)

Band	Reference	$\lambda_{\rm eff}$ (μm)	$j + 2.5 \log h$[a] (AB magnitudes)	Notes
FOCA 0.2 μm[b]	Sullivan et al. 2000	0.20	-13.83 ± 0.25	$z \approx 0.15$, uncorrected for dust
APM b_J[c]	Madgwick et al. 2002	0.46	-15.53 ± 0.10	$z \approx 0.10$
	Norberg et al. 2002	0.46	-15.43 ± 0.10	Evolution corrections to $z = 0.0$
SDSS $^{0.1}u$[d]	Blanton et al. 2003b	0.32	-14.10 ± 0.15	Evolution corrections to $z = 0.1$
SDSS $^{0.1}g$	Blanton et al. 2003b	0.42	-15.18 ± 0.05	Evolution corrections to $z = 0.1$
SDSS $^{0.1}r$	Blanton et al. 2003b	0.56	-15.90 ± 0.05	Evolution corrections to $z = 0.1$
SDSS $^{0.1}i$	Blanton et al. 2003b	0.68	-16.24 ± 0.05	Evolution corrections to $z = 0.1$
SDSS $^{0.1}z$	Blanton et al. 2003b	0.81	-16.56 ± 0.05	Evolution corrections to $z = 0.1$
2MASS J[e]	Cole et al. 2001	1.24	-16.58 ± 0.15	Evolution corrections to $z = 0.0$
2MASS K_s	Cole et al. 2001	2.16	-16.82 ± 0.15	Evolution corrections to $z = 0.0$
	Kochanek et al. 2001	2.16	-16.94 ± 0.15	$z \approx 0.03$
Hawaii K_s	Huang et al. 2003	2.16	-17.57 ± 0.15	$z \approx 0.15$

[a] Luminosity density conversion: $j = -2.5 \log(L_\nu/{\rm W\ Hz^{-1}\ Mpc^{-3}}) + 34.10$.
[b] FOCA magnitudes: assumed $m_{\rm AB} = m_{2000} + 2.25$ (Milliard et al. 1992).
[c] APM magnitudes: assumed $m_{\rm AB} = b_J - 0.08$ (see § 2.2).
[d] SDSS magnitudes: assumed $m_{\rm AB} = (u, g, r, i, z) + (-0.04,\ 0.035,\ 0.015,\ 0.015,\ 0.00)$ (Blanton et al. 2003b).
[e] 2MASS, Hawaii magnitudes: assumed $m_{\rm AB} = J + 0.9$, $m_{\rm AB} = K + 1.8$ (see footnote 2).

up spectroscopy is also included as part of the SDSS for various targeting schemes, of which the main galaxy sample (MGS; Strauss et al. 2002) is appropriate for determining cosmic luminosity densities. The MGS is a magnitude-limited galaxy sample ($r < 17.77$) with a median redshift of 0.10. To form effectively complete samples in the other four bands, galaxies were selected to

$$(u, g, i, z) \lesssim (18.4,\ 17.65,\ 16.9,\ 16.5)\ .$$

The first luminosity densities from the MGS were published by Blanton et al. (2001). However, Wright (2001) found that these results overpredicted the near-IR luminosity density by a factor of 2.3 (compared with Cole et al. 2001 and Kochanek et al. 2001). Since then, better analysis techniques, better calibration, and more data have significantly improved the optical luminosity density measurements. We use the results of Blanton et al. (2003b) as the basis for our fitting here. One of their approaches was to k-correct and to evolve-correct to a fiducial redshift of 0.10. This reduces systematic uncertainties associated with these types of corrections because the median redshift of the SDSS is at this mark and the luminosity-weighted mean redshift is close to it. Thus, their results are most accurate for the shifted bandpasses, designated ${}^{0.1}u$, ${}^{0.1}g$, ${}^{0.1}r$, ${}^{0.1}i$, and ${}^{0.1}z$ (rest-frame bandpasses for galaxies at $z = 0.1$). We use the ${}^{0.1}r$ band as the fiducial band and measure all colors with respect to it when comparing synthetic magnitudes with luminosity densities. We set a 1 σ uncertainty of 0.05 for the g-, r-, i-, and z-band measurements. This allows for some miscalibration since the formal uncertainties of Blanton et al. are 0.03/0.02 for these bands. Using such small errors is appropriate since it is the measurement of ${}^{0.1}g$, ${}^{0.1}i$, and ${}^{0.1}z$ relative to ${}^{0.1}r$ that constrains the normalized SFH or IMF. In other words, the errors need only to represent the uncertainties in the colors, and the absolute measurements of the luminosity densities need not be accurate to this level. An estimated conversion of SDSS to AB magnitudes is given and used by Blanton et al. (see also Table 1), and the magnitudes used by them are assumed to be close enough to total that a correction is not applied.

The new results of Blanton et al. (2003b) are in good agreement with b_J luminosity densities determined by Madgwick et al. (2002) and Norberg et al. (2002). These analyses were based on the Automated Plate Measuring (APM; Maddox et al. 1990) galaxy catalog with redshifts from the Two-Degree Field Galaxy Redshift Survey (2dFGRS; Colless et al. 2001). The conversion to AB magnitudes of -0.08 was based on an integration of the b_J curve (P. C. Hewett & S. J. Warren 1998, private communication) through a spectrum of Vega (Lejeune, Cuisinier, & Buser 1997, computed by R. L. Kurucz). The b_J magnitudes were calibrated to total by comparison with deeper, CCD photometry.

2.3. *Infrared:* 1.0–2.5 μm

The Two Micron All Sky Survey (2MASS; Skrutskie et al. 1997) has imaged the whole sky in the J, H, and K_s bands to a depth of 15–16 AB magnitudes (14.7, 13.9, 13.1 Vega magnitudes, respectively). Cole et al. (2001) matched the second incremental data release to redshifts obtained by the 2dFGRS. With this data set, they determined the local J- and K-band luminosity functions. With k and evolution corrections to $z = 0$, the Schechter parameters were (-22.36, 0.0104, -0.93) and (-23.44, 0.0108, -0.96) for the J and K bands, respectively. Integrating these functions gives -17.36 and -18.50. The conversions to AB magnitudes are taken as $m_{\rm AB} = J + 0.9$ and $K + 1.8$, and the conversion to total magnitudes is estimated to be between -0.08 and -0.15 (we take -0.12).[2] The uncertainties come from Poisson noise, the absolute calibration, the conversion to total magnitudes, and large-scale structure. These are not all well defined, but we will be conservative and use 0.15 for the 1 σ uncertainty so that

$$j = -16.58 \pm 0.15 \quad \text{and} \quad j = -16.82 \pm 0.15$$

for the J and K bands, respectively.

The K-band luminosity function was also determined by Kochanek et al. (2001), using 2MASS imaging. Here they determined the luminosity density using a shallower sample but one with greater sky coverage for the redshifts. Their best estimate was obtained by summing separate luminosity functions for late and early-type galaxies: (-22.98, 0.0101, -0.87) and (-23.53, 0.00 45, -0.92). The total luminosity density is then -16.94 in AB magnitudes after appropriate corrections (to AB, as above; to total, -0.21). This is in good agreement with the Cole et al. result.

A deeper K-band survey, covering about 8 deg^2, was recently analyzed by Huang et al. (2003). Imaging was taken with the University of Hawaii telescopes at Mauna Kea Observatory (Huang et al. 1997), and redshifts were obtained using the 2dF facility on the Anglo-Australian Telescope. The best-fit Schechter parameters were (-23.70, 0.0130, -1.37), giving a luminosity density of $j = -17.57$ after correcting to AB magnitudes. Even with a conservative error of 0.15, this result is greater than 3 σ discrepant from the result of Cole et al. (2001). This discrepancy of 0.75 mag is too large to be explained by cosmic evolution since the K-band luminosity density is dominated by the older stellar populations. Analysis by Huang et al. (2003) suggests that it could be due to a local underdensity. We note that near-IR luminosity densities have larger uncertainties due to large-scale structure than bluer measurements. In underdense regions, the SFR per galaxy is higher (as noted by color-density and morphology-density relationships; e.g., Blanton et al. 2003a), which counteracts the effect on the UV luminosity density.

Given the above discrepancy in the near-IR luminosity densities, we will first consider the Cole et al. results separately from the Huang et al. results in our fitting, and then we will use an average K-band luminosity.

3. MODELING

We fit the data with synthetic magnitudes calculated using the PEGASE.2 evolutionary synthesis code (Fioc & Rocca-Volmerange 1997)[3] and integrating the spectra through the filter response curves (Fig. 3). The responses for the SDSS are taken from Stoughton et al. (2002), the FOCA filter curve is assumed to be Gaussian (Milliard et al. 1992), and the near-IR filter curves are taken from R. M. Cutri

[2] See R. M. Cutri et al. 2001, Explanatory Supplement to the 2MASS Second Incremental Data Release (IPAC/Caltech) at http://www.ipac.caltech.edu/2mass/releases/second/doc/explsup.html.

[3] Revised 2001 May. PEGASE.2 is available at http://www.iap.fr/users/fioc/PEGASE.html.

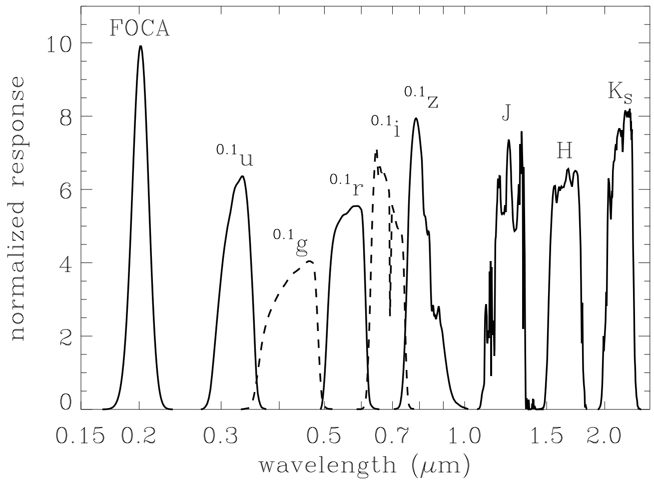

FIG. 3.—FOCA, SDSS, and 2MASS filters. The SDSS filters are shown "shifted" to $z = 0.1$ since we are fitting to the results of Blanton et al. (2003b). Each curve is normalized so that the integral of the normalized transmission $T d \ln \lambda$ is equal to unity. Thus the height of each curve is related to its resolving power ($\lambda/\Delta\lambda$).

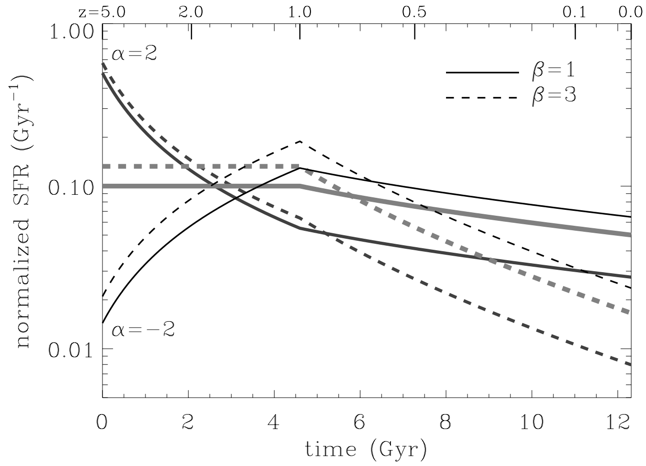

FIG. 4.—Examples of the parameterized cosmic SFH. The SFR is proportional to $(1+z)^\beta$ for $z < 1$ and $(1+z)^\alpha$ for $1 < z < 5$. Each curve is normalized so that the total star formation between $z = 5$ and $z = 0$ is unity. The timescale is for $(h, \Omega_{m_0}, \Omega_{\Lambda_0}) = (0.7,\ 0.3,\ 0.7)$. Six SFHs are shown with two values of β (1, 3) for each of three values of α (−2, 0,2).

et al. (see footnote 2). We run the PEGASE models with nebular emission but "no extinction," except we modified the code so that the absorption of Lyman continuum photons by dust was still included (following the prescriptions of Spitzer 1978). This was done because our dust attenuation parameterization (§ 3.4) does not apply to this "preextinction" of nebular continuum and line emission. The prescription for the models is described below including SFH, IMF, and chemical evolution. We include further effects of dust attenuation on the output spectra.

3.1. *Cosmic SFH*

For our modeling of cosmic star formation history we use a "double power-law" parameterization (Baldry et al. 2002):

$$\mathrm{SFR} \propto \begin{cases} (1+z)^\beta & \text{for } 0 < z < 1\ , \\ (1+z)^\alpha & \text{for } 1 < z < 5\ . \end{cases} \quad (2)$$

The SFRs from the two power laws are the same at $z = 1$, and star formation is started at $z = 5$. Clearly, there are many other possible cosmic SFHs other than defined by these two parameters. However, the resulting synthetic spectra are highly degenerate with SFH. We chose this two-parameter model because the β parameter provides a good match to direct measures of SFR at $z \lesssim 1$ and the α parameter allows us to add high-redshift star formation in a well-defined way. We assume a cosmology corresponding to $(h, \Omega_{m_0}, \Omega_{\Lambda_0}) = (0.7,\ 0.3,\ 0.7)$. Most importantly, this determines the timescale for cosmic SFH measurements.

Examples of this parameterized cosmic SFH are shown in Figure 4 with a timescale for the $h = 0.7$ cosmology. Note that direct measures of the *relative* cosmic SFH with redshift do not depend on H_0. The Hubble constant changes the scaling factor at all redshifts by the same amount. However, our modeling of the cosmic SFH, to fit to local luminosity densities (fossil cosmology), does depend on H_0 because of the timescale dependence. The synthetic spectra are calculated at 11 Gyr, corresponding to the fiducial redshift, $z = 0.1$, with the chosen cosmology and $z_{\rm form} = 5$.

There is overwhelming evidence for a rise in SFR to $z = 1$ from a variety of indicators (e.g., Haarsma et al. 2000; Hammer et al. 1997; Lilly et al. 1996; Rowan-Robinson et al. 1997). Recent estimates from compilations of measures of luminosity density with redshift out to $z = 1$ give, for example, $\beta = 2.7 \pm 0.7$ (Hogg 2002). If we take the formal 2 σ range from Hogg, we obtain a range of 1.3–4.1. However, some of the measurements compiled by him could be biased toward a steeper evolution (e.g., Lilly et al.) because of selection effects. Cowie, Songaila, & Barger (1999) found a shallower evolution of $\beta = 1.5 \pm 0.5$ on the basis of rest-frame UV selection at all redshifts. To encompass the "evidence for a gradual decline" (Cowie et al.) to a steep decline (Lilly et al.), we will consider β to be in the range 0.5–4.0.

High-redshift ($z > 1$) star formation is parameterized by α and $z_{\rm form} = 5$. We do not try to exactly match high-redshift measurements. The uncertainties are still large because of , for example, dust and surface brightness corrections. By taking α from −2 to 2, we can approximate the effect of high-redshift star formation, which could range from a rapid decline at high redshift (Madau et al. 1996), to a flattening (Steidel et al. 1999), to a rapid rise (Lanzetta et al. 2002). Note that the effect of any significant star formation in the ~1 Gyr between $z = 20$ and $z = 5$ can be approximated by an increase in α.

3.2. *Universal IMF*

Significant degeneracies exist with modeling the spectra of galaxies, e.g., age-metallicity. Given these uncertainties, modelers have generally assumed an IMF, typically the Salpeter (1955) IMF, for modeling galaxy spectra. Here we will assume a universal IMF (constant with time and environment) but we will consider different IMF power-law slopes. A double power-law IMF is chosen on the basis of the rationale that there is a clear change in slope around 0.5 $M_\odot$ but no definitive change at higher masses (Kroupa

2001). Our parameterization[4] is

$$n_{\log m} \propto \begin{cases} m^{-0.5} & \text{for } 0.1 < m < 0.5 \ , \\ m^{-\Gamma} & \text{for } 0.5 < m < 120 \ , \end{cases} \qquad (3)$$

where $n_{\log m} d \log m$ is the number of stars with logarithm of the mass in the range $\log m$ to $\log m + d \log m$ and m is in units of solar masses with 0.1 and 120 $M_\odot$ being the IMF cutoffs. For the Salpeter (1955) IMF, $\Gamma = 1.35$ in this formalism, except that traditionally the slope continues down to 0.1 $M_\odot$. A comparison between different IMFs is shown in Figure 1. Note that despite the average IMF of Scalo (1998) using a break at 1 and 10 $M_\odot$, Figure 5 of that paper appears consistent with a single break at 0.5–0.8 $M_\odot$. Thus, as with Kroupa (2001), there is no strong evidence to rule out a double-power law IMF with a break at 0.5 $M_\odot$ being an adequate approximation of a universal IMF. For the low-mass slope, we use the average of the two Kroupa equations. We do not vary this slope since our results are less sensitive to this than the upper mass slope.

3.3. *Chemical Evolution*

For chemical evolution, we incorporate the closed-box evolutionary model within PEGASE, which uses the models of Woosley & Weaver (1995) to estimate metallicity production via supernovae. The metallicity is controlled by a parameter r (Baldry et al. 2002) that represents the total mass of stars formed between $z = 5$ and $z = 0$ divided by the total amount of gas initially available. Higher values of r produce higher metallicity. The parameter can be greater than unity because of recycling of material. Since we are comparing different IMFs, we do not quote r values but rather the value for the metallicity ($\bar{Z}$) averaged on the luminosity at $z = 0.1$ (the $\bar{Z}$-r dependence varies with IMF). Solar metallicity is considered to be $Z = 0.02$ in the PEGASE models.

3.4. *Dust Attenuation*

We wish to estimate the effective dust attenuation for the cosmic spectrum covering the UV to near-IR. However, we cannot consider a standard slab or screen model as we would for an individual galaxy because the contributions to the luminosity densities come from many types of galaxies. Kochanek et al. (2001) estimated 54% and 46% contributions to the K band from late- and early-type galaxies, respectively. The ratio is similar in the visible red bands from the SDSS survey, although it depends on the chosen dividing line in color or morphology (Blanton et al. 2003a). From Madgwick et al. (2002), 61% and 39% are the fractional contributions to the b_J band from late and early types, respectively, based on spectroscopic classification (assuming spectral types 2–4 for late, type 1 for early). Late-type galaxies (Sa–Sd and starbursts) contribute about 90%–95% of the light in the 0.2 μm UV (estimated from Table 7 of Sullivan et al. 2000). This is consistent with the results obtained by Wolf et al. (2003) for the 0.28 μm UV at $z = 0.3$, with about 75%/90% contribution from late spectral types (3–4/2–4). Using the inclination-averaged attenuations of various galaxy types given by Calzetti (2001, Table 3) and averaging over suitable distributions at each wavelength, we obtain cosmic spectrum attenuations in magnitudes of 1.1–1.35 at 0.15 μm, 0.4–0.55 at 0.45 μm, 0.2–0.3 at 0.8 μm, and 0.05–0.1 at 2.2 μm.

To incorporate dust attenuation, we use a power law. The attenuation in magnitudes as a function of wavelength is approximated by

$$A_\lambda = A_v \left(\frac{\lambda}{\lambda_v} \right)^{-n} , \qquad (4)$$

where A_v is the attenuation at the fiducial wavelength of λ_v. We use 0.56 μm since it matches the effective wavelength of our fiducial $^{0.1}r$ band and is close to the standard V band (0.55 μm).

If we fit to the cosmic spectrum attenuations, estimated above, we obtain $(A_v, n) \approx (0.35, \ 1.0)$ for our fiducial dust model. This curve is within the ranges in attenuation estimated above at each wavelength. Charlot & Fall (2000) found that for an average starburst galaxy, n was approximately 0.7 in a UV-to-visible attenuation law. Their model also included increased effective absorption in birth clouds, which had a finite lifetime. Here we assume that the average of all galaxies (the luminosity densities considered here) can be approximated by a single effective optical depth. The average spectrum of the universe is not that of a starburst galaxy, and the broadband colors are not strongly affected by emission lines. The luminosity density attenuations are naturally steeper than $n = 0.7$ because of the increasing contribution of less dusty ellipticals as the wavelength is increased. Rather than restricting our fitting to a single value of n, we allow for a range from 0.8 to 1.2.

For A_v, we allow for a range from 0.2 to 0.55 mag. For $n = 1.0$, this is equivalent to a range in A_{2000} from 0.55 to 1.55 mag. This encompasses the difference between the uncorrected and dust-corrected luminosity densities of Sullivan et al., which amounts to 1.3 mag. To avoid excessive attenuation at UV and near-IR wavelengths, we also set $0.5 \leq A_{2000} \leq 1.6$ and $A_K \leq 0.15$, which reduces the A_v range away from $n = 1.0$. In general, we marginalize over attenuation, i.e., we chose the best-fit parameters within the defined ranges that minimize χ^2 when fitting the SFH and IMF.

3.5. *Summary of Parameters*

In this section we summarize the important parameters and ranges considered in our analysis and show the effect of varying some of the parameters.

(1) *Synthetic spectra.*—PEGASE.2 (Fioc & Rocca-Volmerange 1997; see also footnote 3): Padova tracks (Bressan et al. 1993), and spectral libraries of Lejeune et al. (1997) and Clegg & Middlemass (1987). The Lejeune et al. library is principally derived from Kurucz (1992) model atmospheres. Nebular continuum and line emission is also included.

(2) *Cosmology.*—We use $(h, \Omega_{m_0}, \Omega_{\Lambda_0}) = (0.7, \ 0.3, \ 0.7)$ (except luminosity densities are quoted for $h = 1$, or, equivalently, as $j + 2.5 \log h$). These values are fixed in our analysis.

(3) *Cosmic SFH.*—See § 3.1 and equation (2). We use β in the range [0.5, 4.0], α in the range [−2, 2], and $z_{\rm form} = 5$. Low-redshift ($z < 1$) star formation is parameterized by SFR $\propto (1+z)^\beta$ and high-redshift by $(1+z)^\alpha$.

[4] An equivalent formalism for our upper mass slope is $dN/d \log m \propto m^{-\Gamma}$, where N is the cumulative number of stars up to mass m. This follows the nomenclature outlined by Kennicutt (1998).

(4) *Universal IMF.*—See § 3.2 and equation (3). We use power-law slopes of -0.5 (for $m < 0.5\ M_\odot$) and $-\Gamma$ in the range $[-0.8,\ -1.8]$ (for $m > 0.5\ M_\odot$) with $(m_{\rm min}, m_{\rm max}) = (0.1,\ 120)$. The power laws are with respect to $\log m$ so that the Salpeter IMF slope is -1.35.

(5) *Chemical evolution.*—See § 3.3. We use a closed-box approximation with $\bar{Z}$ in the range [0.008, 0.05] ($Z_\odot = 0.02$) from r between [0.1, 1.4]. The final luminosity-weighted metallicity $\bar{Z}$ is principally a function of r and the IMF.

(6) *Dust attenuation.*—See § 3.4 and equation (4). We use a power-law slope of $-n$ in the range $[-0.8, -1.2]$ with A_v in the range [0.2, 0.55]. The ranges are also constrained by $0.5 \leq A_{2000} \leq 1.6$ and $A_K \leq 0.15$.

Figure 5 shows the effects of varying one parameter on the synthetic spectra (normalized at the ${}^{0.1}r$ band) with respect to a model of

$$(\Gamma, \beta, \alpha, \bar{Z}, A_v, n) = (1.3,\ 2.5,\ 0,\ 0.018,\ 0.35,\ 1.0)\ .$$

Over our chosen parameter ranges, varying the IMF slope Γ has the largest effect on the UV$-{}^{0.1}r$ colors, with β having the second largest effect. The metallicity has the largest effect on the near-IR $-\ {}^{0.1}r$ colors.

4. RESULTS

First, we fit to the UV-to-optical luminosity density measurements of Sullivan et al. (2000) and Blanton et al. (2003b), with different near-IR measurements: (1) with the Cole et al. (2001) K-band result (the compilation is designated SBC_K), (2) with the Huang et al. (2003) result (compilation SBH), and (3) with the Cole et al. J-band result (compilation SBC_J), which did not include the z-band measurement included in the first two compilations. Examples of fitted spectra are shown in Figure 6. This shows that the near-IR luminosity density measurements can be fitted, primarily by varying metallicity, while the UV-to-optical spectrum remains approximately the same. Within the range of metallicity considered here (0.4–2.5 $Z_\odot$), the best fit is obtained to the SBC_K data. Here all the measurements are within about 1 σ of the synthetic magnitudes. The new results of Blanton et al. (2003b) and this analysis resolves the major discrepancy noted by Wright (2001) between the optical and near-IR luminosity densities. However, there is a significant discrepancy between the Hawaii and the 2MASS K-band luminosity densities and a discrepancy between the J-band result and the z-band/K-band results.

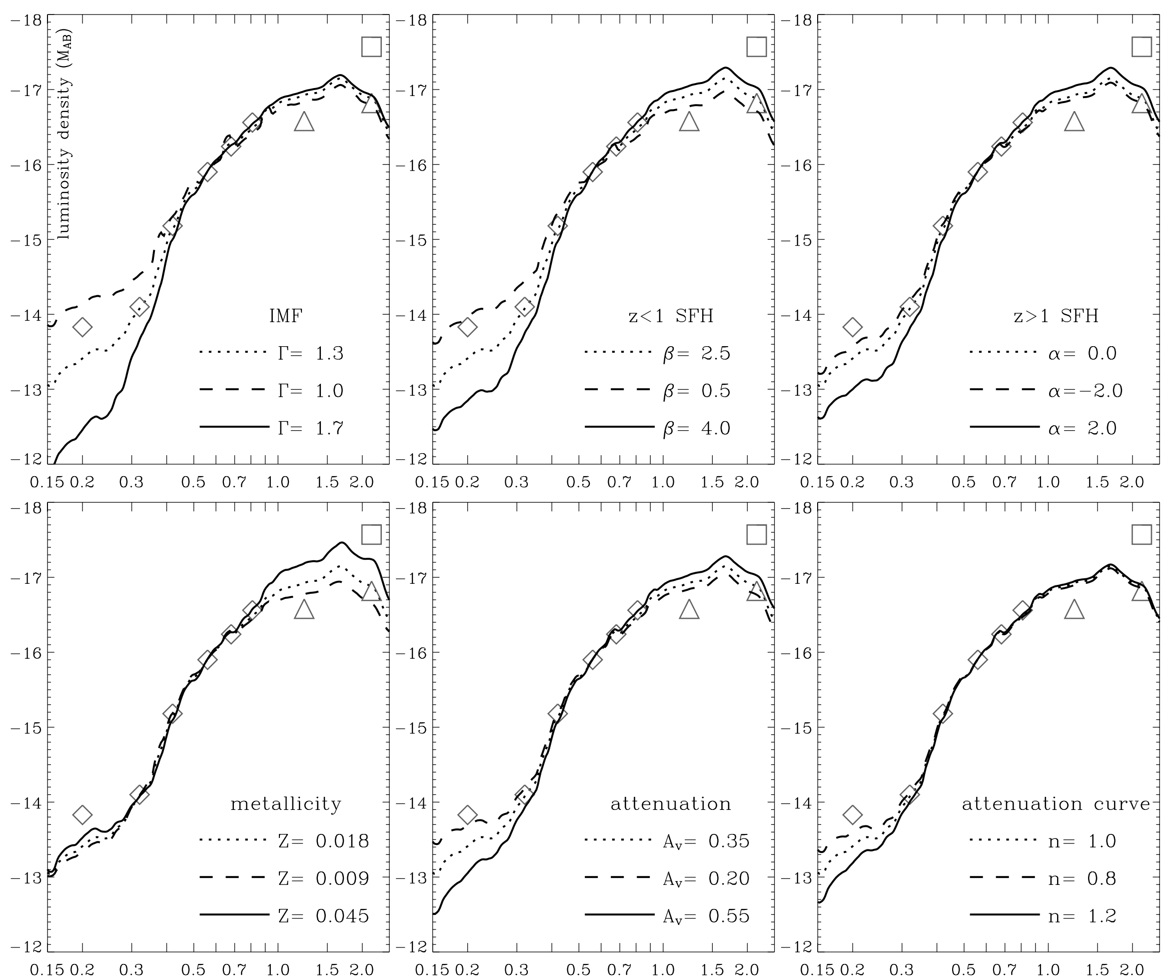

FIG. 5.—Effect of varying selected parameters individually: absolute magnitude vs. wavelength. The lines represent synthetic spectra smoothed to $\lambda/\Delta\lambda \sim 10$. The dotted line is derived from the same set of parameters in every panel $[(\Gamma, \beta, \alpha, \bar{Z}, A_v, n) = (1.3,\ 2.5,\ 0,\ 0.018,\ 0.35,\ 1.0)]$. All the spectra are normalized to -15.90 in the ${}^{0.1}r$-band filter (Blanton et al. 2003b). The symbols represent luminosity density measurements: the diamonds are for Sullivan et al. (2000) and Blanton et al. (2003b), the triangles are for Cole et al. (2001), and the square is for Huang et al. (2003).

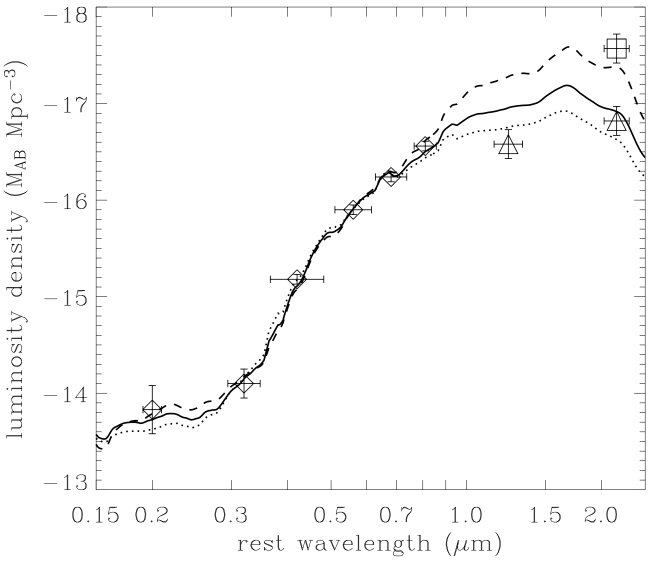

FIG. 6.—Example fits to data from SBC_K (UV, *ugriz*, and *K* triangle; *solid line*), SBH (UV, *ugriz*, and *K* square; *dashed line*) and SBC_J (UV, *ugri*, and *J*; *dotted line*). The lines represent the fitted synthetic spectra smoothed to $\lambda/\Delta\lambda \sim 10$. The parameters for these fits were $(\Gamma, \beta, \alpha, \bar{Z}, A_v, n) =$ (1.1, 4.0, 0, 0.022, 0.20, 0.9) for SBC_K, (1.1, 3.5, 0, 0.048, 0.44, 0.8) for SBH, and (1.1, 4.0, 0, 0.009, 0.22, 0.8) for SBC_J. See text for details.

Neither of the infrared surveys is ideal for comparison with the SDSS survey results. The 2MASS survey is too shallow (median $z \sim 0.05$ at the limit of the extended source catalog) for direct comparison with the $z = 0.1$ analysis, and the Hawaii survey goes deeper but has a significantly smaller area (8 deg^2). Note that the Sullivan et al. result only uses about 200 galaxies, but it is consistent with the $^{0.1}u$-band result. Improved surveys are needed to resolve the near-IR luminosity density discrepancies and to reduce the uncertainties in UV luminosity densities.

We first look at constraints on the metallicity and IMF for a given cosmic SFH (marginalizing over dust attenuation). We compute χ^2 and determine the confidence levels of $\Delta\chi^2 = (1.0,\ 2.3,\ 6.2,\ 11.8)$ corresponding to (68.3%) one-parameter and (68.3%, 95.4%, 99.73%) two-parameter confidence limits. The resulting contours are shown in Figure 7 for a cosmic SFH with $\beta = 2.5$ and $\alpha = 0$ (Hogg 2002; Steidel et al. 1999). As expected, the best-fit metallicity is dependent on the near-IR data: the SBC_K data has a best-fit metallicity around 1–1.5 $Z_\odot$, the SBH data at greater than 2 $Z_\odot$, and the SBC_J data at less than 1 $Z_\odot$. The SBC_K set of data is in agreement with solar neighborhood measurements of the metallicity, which give an average close to solar (Haywood 2001). The SBH data is in disagreement with solar metallicity at the 99.7% confidence level.

For the rest of the paper, we use an average estimate of the *K*-band luminosity corresponding to

$$j = -16.88 \pm 0.25 \qquad (5)$$

from Cole et al. (2001) and Kochanek et al. (2001). The uncertainty was increased, and the *J* band was not included, so the constraints on the IMF were not dependent on the discrepancies noted above. This 1 σ range in the *K*-band luminosity density is also similar to the range determined by Bell et al. (2003). The metallicity-IMF contours for this data set (the compilation is designated SBav) are also shown in Figure 7. The best-fit IMF slope, $\Gamma = 1.3 \pm 0.1$, shows the tightness of the constraint if the SFH is known. The best-fit metallicity is greater than solar, but for other cosmic SFHs (e.g., $\beta = 2.5$ and $\alpha = 2$), the best fit is around solar. In general, there is minimal degeneracy between Γ and metallicity for the data, i.e., the choice of metallicity does not significantly affect the constraints on the IMF slope.

Note that there is an upper limit on the metallicity as a function of Γ due to the closed-box model (Fig. 7). Insufficient metals can be produced in the available time to raise the average metallicity above a certain limit, and this limit decreases as the fraction of high-mass stars in the IMF

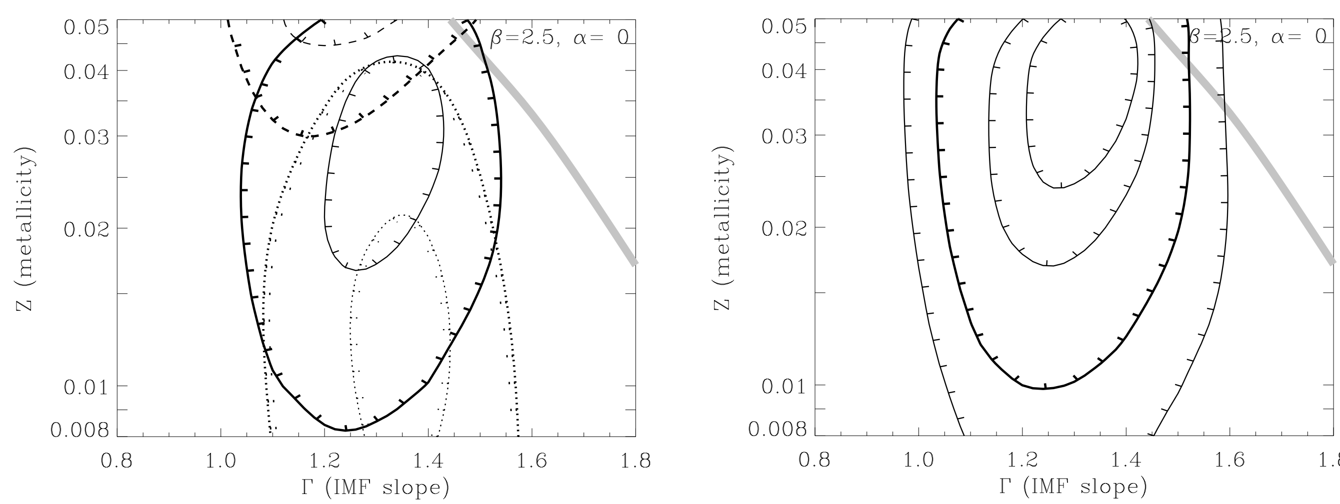

FIG. 7.—Joint confidence levels over metallicity and IMF slope assuming a cosmic SFH ($\beta = 2.5$, $\alpha = 0$). *Left:* The contours represent confidence levels for the SBC_K data (*solid lines*), SBH data (*dashed lines*), and SBC_J data (*dotted lines*). The levels correspond to 68% one-parameter and 95% two-parameter confidence limits, marginalized over dust attenuation. The thick gray line represents the approximate upper limit on the luminosity-weighted $\bar{Z}$ due to chemical evolution (from the closed-box model of PEGASE). Any χ^2 values above this line are linearly extrapolated. *Right:* The same, except that the confidence limits are for the SBav data, which use an average near-IR luminosity estimate (eq. [5]), and the levels represent the 68% one-parameter and 68%, 95%, and 99.7% two-parameter confidence limits.

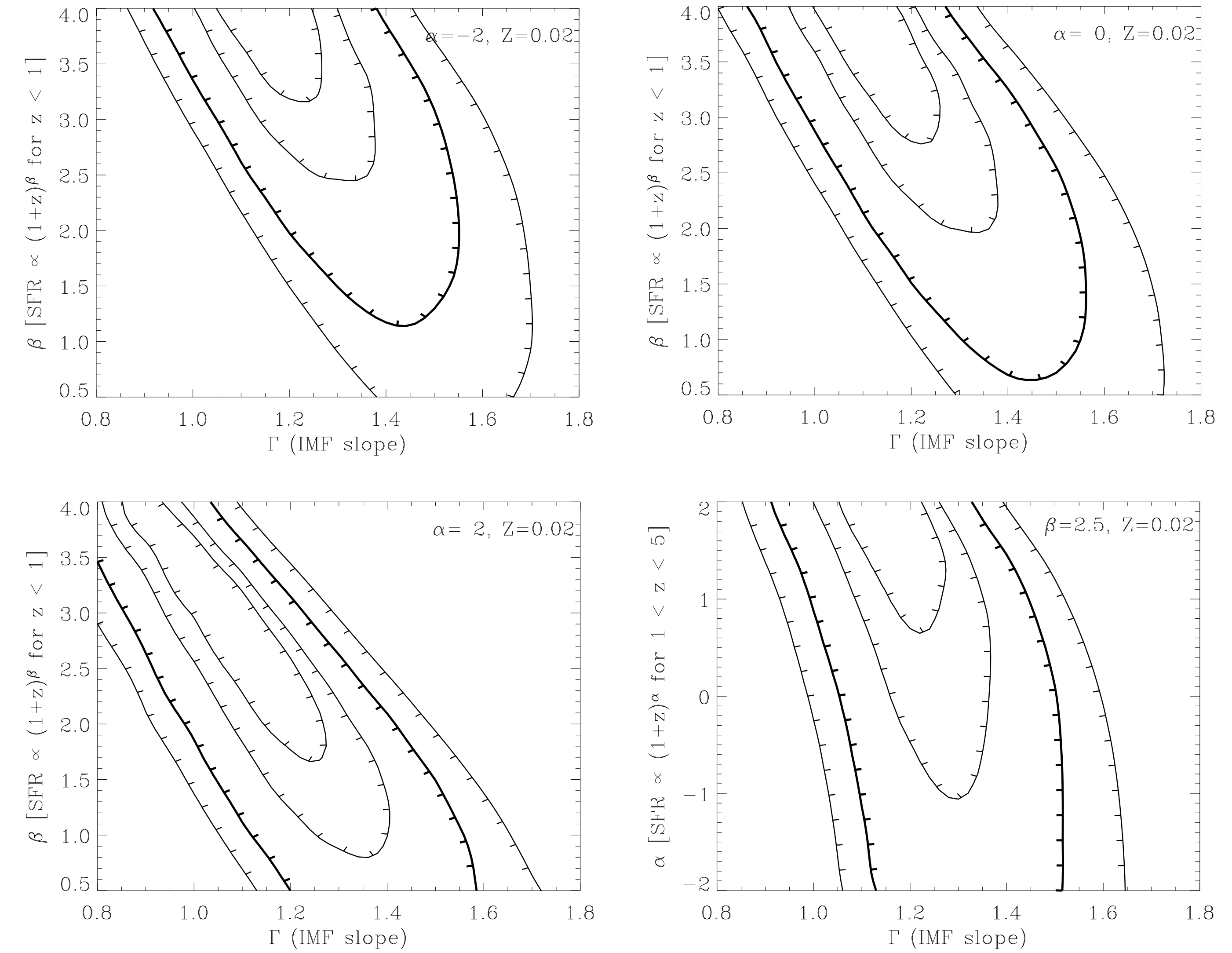

FIG. 8.—Joint confidence levels over β/α and IMF slope for three different values of α (-2, 0, 2) and one value of β (2.5), assuming for a chemical evolution closed-box approximation with $\bar{Z} = 0.02$. The contours represent 68% one-parameter and 68%, 95%, and 99.7% two-parameter confidence levels for the SBav data, marginalized over dust attenuation.

decreases. This chemical evolution limit is derived from the PEGASE code using the upper yields of Woosley & Weaver (1995).

The pattern shown in Figure 7 is similar as β is varied except that the best-fit Γ shifts. To illustrate this, we now fix $\bar{Z}$ equal to 0.02 for the SBav fit and show joint confidence levels in β versus Γ in Figure 8. We plot the result for three values of α. All the plots show a broad degeneracy with a slope of -7 ± 1. In other words, the best-fit Γ decreases by about -0.14 for each $+1$ increase in β. Note that the metallicity was chosen to be consistent with the solar neighborhood, so that the closed-box model was valid out to Γ of 1.8 with only minimal extrapolation (see Fig. 7).

The choice of high-redshift star formation (defined by α) makes little difference for the best-fit Γ (Fig. 8). Marginalizing over SFH (β and α), we obtain a best fit for Γ in the range 0.85–1.3 (68% confidence) and a strong upper limit of $\Gamma < 1.7$ (99.7% confidence). This is our principal result. In other words, assuming a declining SFR from $z = 1$ to the present day ($\beta \geq 0.5$), the present luminosity densities, in particular for the UV–optical colors, mean that the upper mass IMF slope cannot be steeper than 1.7. The caveats are (1) that PEGASE evolutionary tracks and stellar spectra be sufficiently accurate, (2) that cosmic SFH can be approximated with the double power law and the look-back time to $z = 1$ is close to 7.7 Gyr, (3) that there is a close to universal IMF with a near unbroken slope above 0.5 $M_{\odot}$, (4) that chemical evolution can be approximated by a single metallicity for each epoch with the metallicity increasing with time (closed-box approximation), (5) that the average effect of dust can be approximated by a power law within the ranges considered, (6) that the Copernican principle, i.e., that we are in no special place in the universe, applies, and (7) that the luminosity density uncertainties can be approximated as Gaussian.

We now turn to look at varying a couple of these assumptions, related to metallicity and dust, in §§ 4.1 and 4.2. In § 4.3 we calculate the stellar mass, SFR and bolometric densities from our models and, in § 4.4 we apply constraints using measurements of Hα luminosity density.

4.1. *Metallicity Approximations*

We have used the "closed-box" approximation for the evolutionary synthesis in the above analysis. This is valid if the dominant star formation at each epoch is taking place in an average chemical environment at that epoch. This scenario could result from complete mixing between different environments. Hot, young stars have a higher metallicity on average than cool, old stars. Another commonly used assumption in evolutionary synthesis is the "constant-metallicity" approximation. This scenario could result from no mixing between environments. The metallicity evolves independently and rapidly in each separate star-forming region, with a characteristic or average metallicity representing all epochs (separate regions) of star formation.

Since the universe has neither complete nor no mixing, something between these two approximations might be expected.[5] Examples of differences between these are shown in Figure 9. Although the effect on the broadband colors depends on the SFH and IMF, the general effect is to increase the UV and near-IR fluxes with respect to the visible fluxes for the constant-Z approximation. This approximation leads to lower metallicities for young/hot stars and higher metallicities for old/cool stars compared with the closed-box evolution scenario (matching $\bar{Z}$ to constant Z).

Some results for the constant-metallicity approximation are shown in Figures 10 and 11 for the SBav data. If we choose solar metallicity, then the results are similar to the closed-box approximation except Γ is in the range 1.05–1.45 (68% confidence) and $\Gamma < 1.7$ at 95% confidence. The latter confidence level holds for $Z \lesssim 0.025$.

Table 2 shows a comparison between different published IMFs with multiple power-law slopes. We use the constant-metallicity approximation for this comparison to avoid the additional complication introduced by metal production in a closed-box model. With this comparison, the Kroupa, Tout, & Gilmore (1993), Miller & Scalo (1979), and Scalo (1986) IMFs are strongly rejected. This is consistent with their average slopes, over 1–10 and 10–120 $M_\odot$, being $\Gamma \geq 1.7$. Note that our modeling cannot strongly distinguish between different slope changes below 1 $M_\odot$.

[5] We do not consider infall or outflow models, which are often considered for individual galaxies.

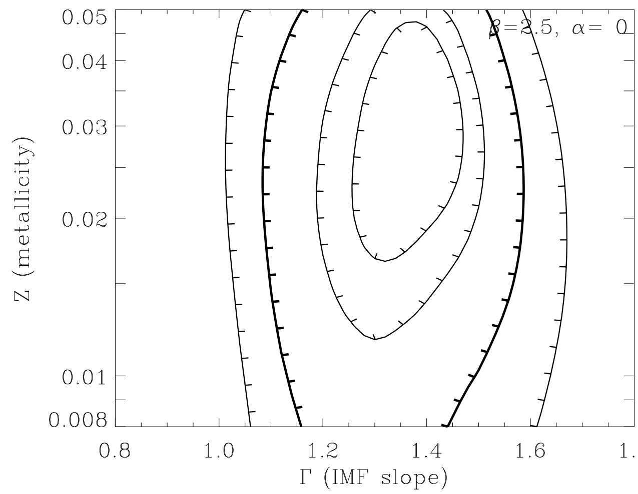

FIG. 10.—Joint confidence levels over metallicity and IMF slope assuming a cosmic SFH ($\beta = 2.5$, $\alpha = 0$) for the constant-metallicity approximation. See Fig. 8 for contour meanings.

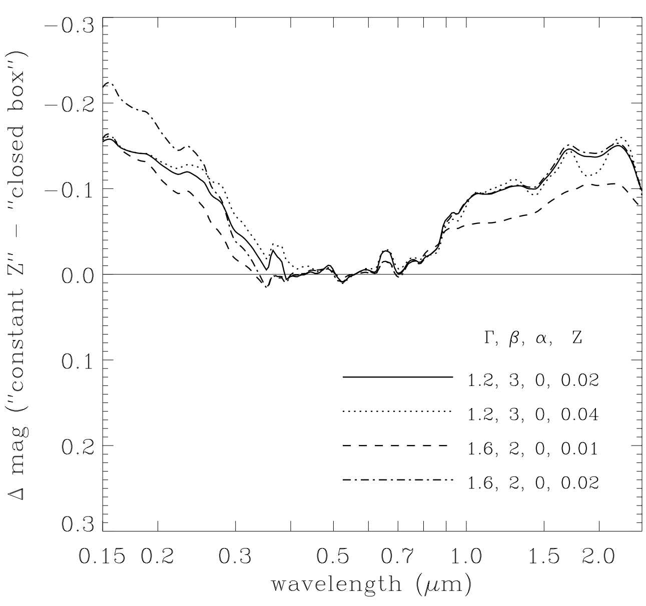

FIG. 9.—Examples of the different effect of constant-Z and closed-box approximations on synthesized colors (with respect to the $^{0.1}r$ band). Both the UV–visible and near-IR–visible fluxes are increased for the constant-Z approximation. The differences are plotted for matching luminosity-weighted $\bar{Z}$ to constant Z.

4.2. *Dust Attenuation Approximations*

We have used a power law to describe average dust attenuation based on estimating the distributions of galaxy types at each wavelength (§ 3.4; $A_v = 0.2$–0.55, $n = 0.8$–1.2). Charlot & Fall (2000) showed that star-forming galaxies were consistent with a shallower or grayer slope of $n = 0.7$. If we take the approximate distribution in the attenuation parameter measured by Charlot et al. (2002), $A_v = 0.8 \pm 0.3$, and we also take $n = 0.7 \pm 0.1$, both with normal distributions (cutoff greater than 0), then the average effective parameters over many galaxies are equivalent to $(A_v, n) \approx (0.75, 0.65)$. In other words, there is a slight reduction in the effective attenuation and a slight flattening of the curve because fluxes are averaged rather than magnitudes. The attenuation for these average parameters at 0.2 μm is 1.45 mag, not far from the average attenuation estimated by Sullivan et al. (2000) of 1.3. Their attenuation corrections were based on Balmer line measurements with conversion to UV attenuation using the Calzetti (1997) law.

In Figure 12 we compare this star-forming galaxy attenuation law (0.75, 0.65) with the average attenuation estimated in § 3.4 (0.35, 1.0) and a steeper MW extinction law ($A_v = 0.5$; Pei 1992). The best-fit regions for these fixed attenuation laws lie primarily within the best-fit region based on marginalizing over metallicity. Thus, our results are not strongly dependent on the assumptions about dust and we have chosen a fairly generous range of parameters for our principal fitting. Note that the grayer law of (0.75, 0.65) produces an unrealistically high attenuation in the K band of 0.3 mag and that the MW extinction law ($n \sim 1.5$ visible–to–near-IR) is naturally too steep because it is a foreground-screen law. In § 4.3 we analyze the consequences

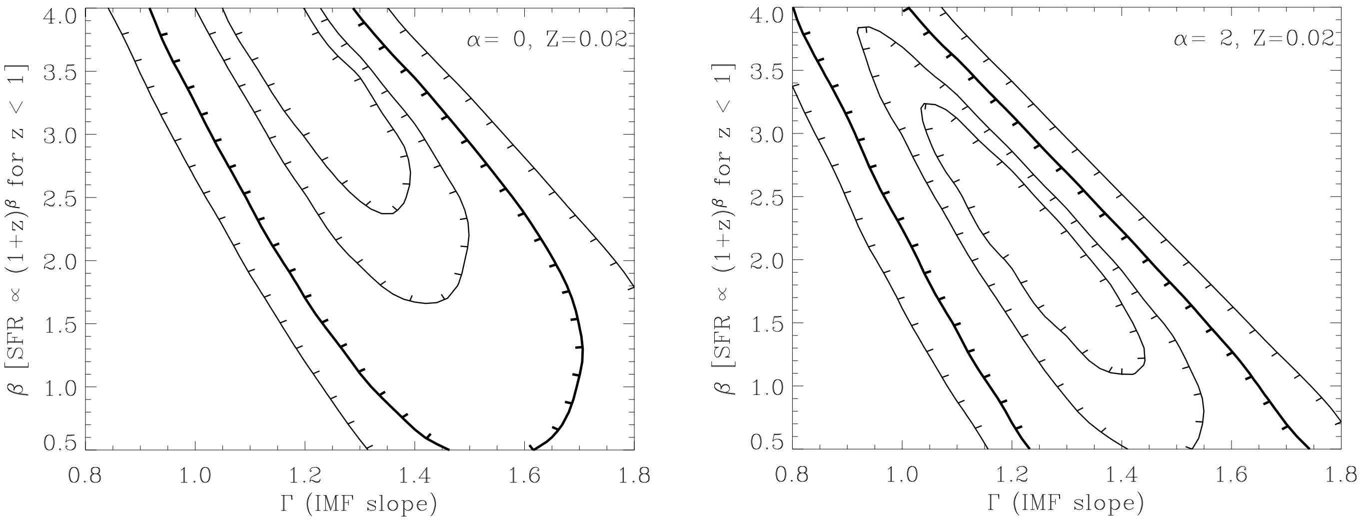

FIG. 11.—Joint confidence levels over β and IMF slope for two different values of α (0, 2), assuming a constant-metallicity approximation with $Z = 0.02$. See Fig. 8 for contour meanings.

of our dust model for IR luminosity density due to dust emission.

4.3. *Stellar Mass, SFR, and Bolometric Densities*

We can calculate some derived physical properties of the universe (at $z \approx 0.1$). The mass density in stars, $\Omega_{\rm stars}$, is in the range $(1.1\text{–}2.0) \times 10^{-3}\ h^{-1}$, and the SFR density, $\rho_{\rm SFR}$, is in the range $(0.7\text{–}4.1) \times 10^{-2}\ h\ M_\odot\ {\rm yr}^{-1}\ {\rm Mpc}^{-3}$. These ranges represent 95% confidence limits marginalized over the IMF and cosmic SFH but restricted to near-solar metallicity models ($\bar{Z}$ or $Z = 0.015$–0.025). However, the results depend strongly on the low-mass end of the stellar IMF, which is not constrained by our analysis. As a test of the varying the low-mass end of the IMF, we also computed the ranges using the best-fitting IMFs and cosmic SFHs described in Table 2 (with less than 95% confidence of rejection). From these, $\Omega_{\rm stars}$ is in the range $(0.8\text{–}2.5) \times 10^{-3}\ h^{-1}$ and $\rho_{\rm SFR}$ is in the range $(1.1\text{–}4.3) \times 10^{-2}\ h\ M_\odot\ {\rm yr}^{-1}\ {\rm Mpc}^{-3}$. The lower stellar mass densities are derived from IMFs with $\Gamma_{m<1} \leq 0.5$ (Kennicutt 1983; Salpeter modified B; Scalo 1998), while the higher mass densities are derived from the Kroupa (2001) model B IMF. The uncertainty in the current SFR density is not increased compared with the measurement based on the equation (3) parameterization. The lowest SFR densities (<0.01) occur only in our models with $\Gamma \lesssim 1.1$, and none of the published IMFs in the table have $\Gamma_{m>1} < 1.2$, which explains the lack of low-SFR densities based on those IMFs.

These results are in good agreement with the results, based on the Kennicutt IMF of Cole et al. (2001) and Baldry et al. (2002), and with the results, based on a modified Salpeter IMF, of Bell et al. (2003). They are generally not in agreement with results based on the Salpeter IMF extending down to $0.1\ M_\odot$ because such an IMF produces a high-mass density from low-mass stars that have minimal impact on the luminosity densities. This type of universal IMF is ruled out by stellar counts in the MW (e.g., Scalo 1986, 1998) and by analysis of the dynamics of spiral galaxies (e.g., Bell & de Jong 2001).

The total bolometric, attenuated, stellar luminosity density (0.09–5 μm) is determined from the models to be in

TABLE 2
COMPARISON AMONG PUBLISHED IMFs

Reference	Power-Law Slopes ($-\Gamma$)[a]				Confidence of Rejection[b] (%)	Best-Fit SFH β (for $\alpha = 0, 2$)
	0.1–0.5 $M_\odot$	0.5–1 $M_\odot$	1–10 $M_\odot$	10–120 $M_\odot$		
This paper	−0.5	−1.2	−1.2	−1.2	<68	3.5, 2.5
Kennicutt 1983	−0.4	−0.4	−1.5	−1.5	80	2.0, 1.0
Kroupa 2001 A	−0.3	−1.3	−1.3	−1.3	<68	3.0, 2.0
Kroupa 2001 B	−0.8	−1.7	−1.3	−1.3	<68	3.0, 2.0
Kroupa et al. 1993	−0.3	−1.2	−1.7	−1.7	98	1.5, 0.5
Miller & Scalo 1979	−0.4	−0.4	−1.5	−2.3	98	1.5, 0.5
Salpeter modified A	−0.5	−1.35	−1.35	−1.35	<68	3.0, 1.5
Salpeter modified B	−0.5	−0.5	−1.35	−1.35	<68	3.0, 2.0
[c]Scalo 1986	−0.15	−1.1	−2.05	−1.5	99.9	0.5, 0.5
Scalo 1998	−0.2	−0.2	−1.7	−1.3	90	1.5, 0.5

[a] All the IMFs are assumed to be valid from 0.1 to 120 $M_\odot$.
[b] The IMFs were compared by marginalizing over 24 SFHs ($\beta = 0.5$–4.0, step 0.5, for $\alpha = -2$, 0, 2) using the constant-metallicity approximation with $Z = 0.02$. The confidence of rejection is with respect to the best-fit IMF in this table.
[c] The power-law slopes shown for the Scalo 1986 IMF are an approximation from a fit to the mass fractions (Fig. 1).

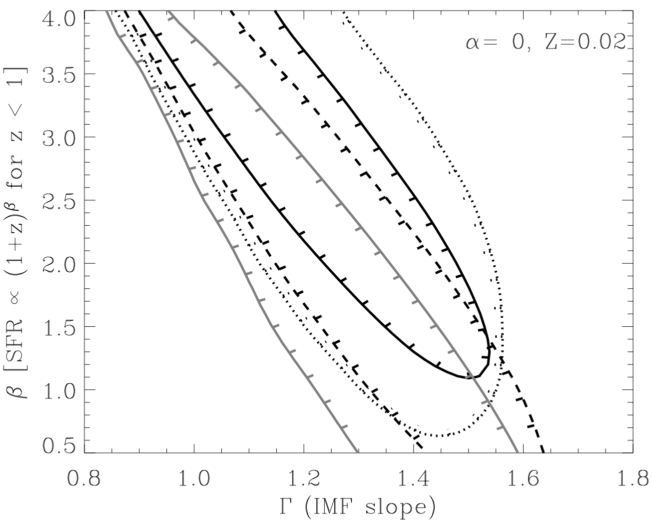

FIG. 12.—Confidence levels in β vs. Γ for various dust approximations with the closed-box approximation. All the contours represent 95% two-parameter confidence limits. The dotted line represents the result from marginalizing over attenuation $A_v = 0.2$–0.55 and $n = 0.8$–1.2 (§ 3.4), the upper solid line from the fiducial $A_v = 0.35$ and $n = 1.0$ (effective average over many galaxies), the dashed line from fixed $A_v = 0.75$ and $n = 0.65$ (star-forming galaxies), and the lower solid line from fixed $A_v = 0.5$ with an MW extinction law (Pei 1992).

the range $(1.2–1.7) \times 10^{35}$ h W Mpc^{-3} (95% confidence). We can also estimate the total, bolometric, luminosity density (∼5–1000 μm) due to dust absorbing and reemitting stellar light. This depends critically on our dust model. From the best-fit models after marginalizing over dust-model parameters, the total is in the range $(0.3–1.5) \times 10^{35}$ h W Mpc^{-3}, which corresponds to 20%–50% of the unattenuated stellar light being absorbed. If we restrict our dust model to $(A_v, n) = (0.35,\ 1.0)$, the ranges are $(0.55–0.95) \times 10^{35}$ h W Mpc^{-3} and 30%–40%.

From Saunders et al. (1990), the local far-IR, 42–122 μm, luminosity density is in the range $(0.17–0.26) \times 10^{35}$ h W Mpc^{-3} ($\pm 2\ \sigma$ range). This is significantly lower than the energy predicted by our dust model. However, a correction to total dust emission needs to be applied. Using the infrared energy dust models of Dale & Helou (2002), corrections from the 42–122 μm band emission to the total dust emission range from 1.9 to 2.6. If we assume that this represents the systematic uncertainty in the luminosity density correction, then the total bolometric dust emission is in the range $(0.3–0.7) \times 10^{35}$ h W Mpc^{-3} (scaling from the Saunders et al. result). Our fiducial dust model has a range in total bolometric emission that overlaps with this estimate.

This upper limit of 0.7×10^{35} h W Mpc^{-3} for the dust emission favors models with lower attenuation and/or lower luminosity densities around 0.2 μm. From our fitting, after marginalizing over dust-model parameters, we obtain $A_{2000} \lesssim 1$. This is marginally inconsistent with the Sullivan et al. (2000) estimate of the effective attenuation, 1.3, which is why we have not used the estimated total dust emission to constrain our dust model. This discrepancy could be resolved if the UV luminosity density and/or attenuation were overestimated,[6] and/or the total IR plus submillimeter flux was underestimated perhaps because of a population of galaxies with colder dust than those detected by 60 μm surveys. Note also that Buat & Burgarella (1998) found an average attenuation of 1.2, but this may not be inconsistent with our attenuation limit since it represents a limit on the luminosity-weighted average by flux. Future analyses could use IR and submillimeter luminosity density measurements to better constrain a dust model.

4.4. Hα *Luminosity Density*

The Hα nebular emission comes from reprocessed Lyman continuum photons. Therefore it provides a measure of the UV flux blueward of 0.1 μm. Here we consider measurements of the attenuation-corrected Hα luminosity density, relative to the $^{0.1}r$ band, in comparison with model predictions. This emission-line attenuation is significantly higher than for the stellar light at the same wavelength (Calzetti, Kinney, & Storchi-Bergmann 1994), but it can be estimated using the Balmer decrement (Hummer & Storey 1987; $H\alpha/H\beta \approx 2.85$ for case B recombination).

Three attenuation-corrected Hα luminosity density measurements are summarized in Table 3. We do not quote error bars because the uncertainties are dominated by systematics. These include (1) subtraction of the stellar contamination, which, in particular, affects the measurement of Hβ and thus the estimate of the attenuation (Glazebrook et al. 2003 included this uncertainty, which amounted to 0.1–0.15 in the log result); (2) uncertainties in the attenuation curve (e.g., Caplan & Deharveng 1986), which affect the conversion from a reddening measurement to absolute attenuation; and (3) AGN contamination. Both the Gallego et al. (1995) and Tresse & Maddox (1998) results are based on obtaining the emission-line luminosity function from spectra. However, the selection criteria of the surveys are different, an emission-line objective-prism survey and *I*-band photometry, respectively. Glazebrook et al. (2003) took the different approach of summing SDSS spectra to form a cosmic optical spectrum before calculating the Hα and Hβ luminosity densities. We take the mean of these three results for our fitting:

$$\log(L_{H\alpha}/h \text{ W Mpc}^{-3}) = 32.63 \pm 0.20 \ . \qquad (6)$$

This is appropriate since the Tresse & Maddox and

[6] However, recent analysis of the FOCA redshift survey with new redshifts and k-corrections gives a slightly more luminous 0.2 μm luminosity density by about 0.2 mag (M. Sullivan 2003, private communication).

TABLE 3
ATTENUATION-CORRECTED Hα LUMINOSITY DENSITIES

Reference	$\log(L_{H\alpha}/h$ W Mpc$^{-3})$	Notes
Gallego et al. 1995	32.39	$z \approx 0.03$, Universidad Comlutense de Madrid objective-prism survey, luminosity function
Tresse & Maddox 1998	32.74	$z \approx 0.20$, Canada-France Redshift Survey, luminosity function
Glazebrook et al. 2003	32.77	$z \approx 0.03$, SDSS, cosmic spectrum

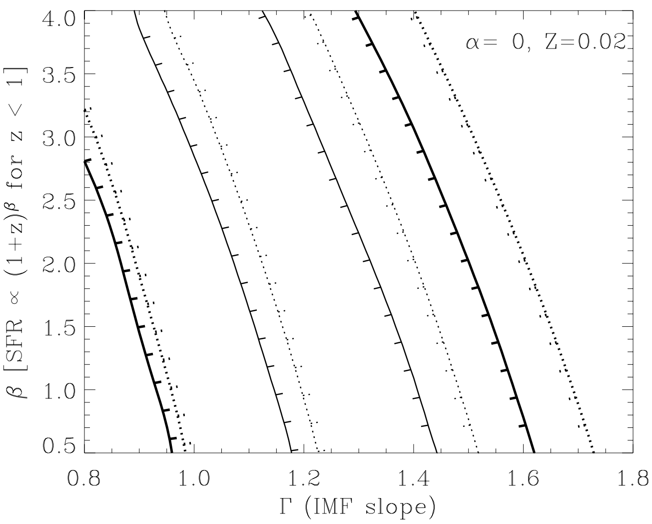

FIG. 13.—Confidence levels in β vs. Γ from fitting solely to the Hα luminosity density (eq. [6], relative to the $^{0.1}r$ band). The solid lines represent the contours for the closed-box approximation, while the dotted lines represent the contours for the constant-metallicity approximation. The contours represent 68% one-parameter and 95% two-parameter confidence levels.

Glazebrook et al. results may be too high because of AGN contamination, which is enhanced by aperture affects. The spectra taken through a fiber are normalized to a broadband filter and since AGN are centrally concentrated, any emission line luminosity due to them will be overenhanced. However, Glazebrook et al. did measure the weak O I λ6300 line, suggesting that the AGN contribution was only a few percent at most. The Gallego et al. result is probably too low because of the small survey (i.e., large-scale structure) and/or because it includes only EW > 10 Å (Hα, emission positive) galaxies.

To compare this average measurement with model predictions, we use the output from PEGASE for the Hα flux without dust attenuation.[7] As with the earlier fitting, the synthetic spectra are normalized to the $^{0.1}r$ band, so we are really comparing the ratio of Hα and $^{0.1}r$-band fluxes between the models and the data. A correction is made for the fact that the measured $^{0.1}r$-band flux includes dust attenuation because we are fitting to an attenuation-corrected Hα measurement. We use the fiducial attenuation of $A_v = 0.35$. In other words, unlike as with the earlier fitting, we now normalize the synthetic spectra to an attenuation-corrected luminosity density in the $^{0.1}r$ band.

Figure 13 shows the results from fitting to the average attenuation-corrected Hα luminosity density. The degeneracy in β versus Γ is similar to that for the broadband luminosity densities. In addition, the best-fit IMF slope, Γ in the range 0.9–1.5 (68% confidence, assuming $\alpha = 0$ and averaging over the metallicity approximations), is in good agreement with the those results.

[7] Some fraction of Lyman continuum photons is assumed to be absorbed by dust rather than gas according to the prescriptions of Spitzer (1978), normalized so that 30% of the photons are absorbed by dust at solar metallicity (see footnote 3).

5. CONCLUSIONS

In this paper, we present the results of fitting spectral synthesis models with varying IMFs to local luminosity densities.

1. A good fit is obtained to the measurements of Sullivan et al. (2000), Blanton et al. (2003b), and the *K*-band measurement of Cole et al. (2001) (compilation SBC_K), with a best-fit metallicity of around solar. If we fit to the measurements of the first two papers and Huang et al. (2003; compilation SBH), the best-fit metallicity is greater than twice solar and the results are inconsistent with solar metallicity at the 99.7% confidence level.

2. The data can be well fitted by a universal IMF, and therefore there is no need to invoke IMF variations. However, this provides only a weak constraint on the invariance of the IMF because of significant degeneracies associated with this type of modeling.

3. The best-fit universal IMF slope marginalized over a significant range of cosmic SFH ($0.5 \leq \beta \leq 4.0$, $-2 \leq \alpha \leq 2$) is $\Gamma = 1.15 \pm 0.2$ based on an average between a closed-box approximation and a constant-metallicity approximation around solar (using compilation SBav). Our results are in good agreement with the Salpeter IMF slope.

4. A strong upper limit of $\Gamma < 1.7$ is obtained with 99.7% or 95% confidence depending on the metallicity approximation. This rules out the Scalo (1986) IMF for a universal IMF since the mass fraction of stars above 10 $M_\odot$ is similar to our parameterization with $\Gamma = 1.8$ (Fig. 1; see also Table 2). A similar conclusion was reached by Madau et al. (1998) from fitting to luminosity densities over a range of redshifts and by Kennicutt et al. (1994) from fitting to Hα EW-color relations for galaxies. Madau et al. found that a Salpeter IMF or an IMF with $\Gamma = 1.7$ provided adequate fits. Here we find that the latter slope does not provide a good fit to luminosity densities. This is principally because we have used more accurate local luminosity density measurements. If we increase our 1 σ uncertainties by 0.05 at all wavelengths, then we obtain $\Gamma < 1.7$ with 80% confidence.

5. The stellar mass density of the universe is in the range $(1.1\text{–}2.0) \times 10^{-3}\ h^{-1}$, based on marginalizing over cosmic SFH and our parameterization of the IMF. The current SFR density is in the range $(0.7\text{–}4.1) \times 10^{-2}\ h\ M_\odot$ yr^{-1} Mpc^{-3}. The total bolometric stellar emission (0.09–5 μm) is known more accurately (naturally, because we observe light and not mass) and is in the range $(1.2\text{–}1.7) \times 10^{35}\ h$ W Mpc^{-3} derived from the fitted PEGASE model spectra (the mass-to-light ratio is ~0.9–1.4 $M_\odot/L_\odot$). We find that our dust model can reproduce the estimated total dust emission [$(0.3\text{–}0.7) \times 10^{35}\ h$ W Mpc^{-3}, ~5–1000 μm] scaled from the far-IR luminosity density (Saunders et al. 1990) if we have $A_{2000} \lesssim 1$ ($\lesssim 60\%$). Note that this represents a limit on the cosmic spectrum attenuation, i.e., a luminosity-weighted average by flux (not magnitude).

6. Fitting to the local Hα luminosity density provides a similar result for the IMF slope ($\Gamma = 1.2 \pm 0.3$). This provides some evidence that our upper mass cutoff of 120 $M_\odot$ is a reasonable approximation because the sensitivity of the Hα flux to massive stars is different from that of the mid-UV to optical fluxes. More accurate measurements could test this upper mass limit.

7. The quantitative results on Γ rely on the accuracy of the population synthesis model (PEGASE). An alternative,

qualitative result would be that there is consistency between the theory of evolutionary population synthesis (evolutionary tracks and stellar spectra) and the measurements of luminosity densities, cosmic SFH, and an average MW IMF derived from stellar counts (e.g., $\Gamma \approx 1.3$, from Kroupa 2001).

Greater constraints can be placed on a universal IMF both by improved accuracy in local luminosity density measurements (in particular, $z = 0.1$ to match the multiwavelength SDSS MGS) and by improved accuracy of direct measures of cosmic SFH with redshift (in particular, $z = 0$ to $z \sim 1$–2). For the direct tracing of cosmic SFH, it is important that the UV is measured at the same rest-frame wavelength in order to avoid IMF dependency. In other words, we need an IMF-independent cosmic SFH in order for the local luminosity densities to accurately constrain a universal IMF or for the IMF dependency to be quantified.

We thank the referee Eric Bell for constructive suggestions and Timothy Heckman, Benne Holwerda, Rosemary Wyse, and Andrew Blain for helpful comments. We acknowledge generous funding from the David and Lucille Packard foundation.

REFERENCES

Baldry, I. K., et al. 2002, ApJ, 569, 582
Barbaro, G., & Poggianti, B. M. 1997, A&A, 324, 490
Bell, E. F., & de Jong, R. S. 2001, ApJ, 550, 212
Bell, E. F., McIntosh, D. H., Katz, N., & Weinberg, M. D. 2003, ApJ, submitted (astro-ph/0302543)
Blanton, M. R., et al. 2001, AJ, 121, 2358
———. 2003a, ApJ, in press (astro-ph/0209479)
———. 2003b, ApJ, 592, 819
Bressan, A., Fagotto, F., Bertelli, G., & Chiosi, C. 1993, A&AS, 100, 647
Buat, V., & Burgarella, D. 1998, A&A, 334, 772
Calzetti, D. 1997, in AIP Conf. Proc. 408, The Ultraviolet Universe at Low and High Redshift, ed. W. H. Waller (Woodbury: AIP), 403
———. 2001, PASP, 113, 1449
Calzetti, D., Kinney, A. L., & Storchi-Bergmann, T. 1994, ApJ, 429, 582
Caplan, J., & Deharveng, L. 1986, A&A, 155, 297
Charlot, S., & Fall, S. M. 2000, ApJ, 539, 718
Charlot, S., Kauffmann, G., Longhetti, M., Tresse, L., White, S. D. M., Maddox, S. J., & Fall, S. M. 2002, MNRAS, 330, 876
Clegg, R. E. S., & Middlemass, D. 1987, MNRAS, 228, 759
Cole, S., et al. 2001, MNRAS, 326, 255
Colless, M., et al. 2001, MNRAS, 328, 1039
Contini, T., Treyer, M. A., Sullivan, M., & Ellis, R. S. 2002, MNRAS, 330, 75
Cowie, L. L., Songaila, A., & Barger, A. J. 1999, AJ, 118, 603
Dale, D. A., & Helou, G. 2002, ApJ, 576, 159
Dey, A., Spinrad, H., Stern, D., Graham, J. R., & Chaffee, F. H. 1998, ApJ, 498, L93
Elmegreen, B. G. 1999, ApJ, 515, 323
Fioc, M., & Rocca-Volmerange, B. 1997, A&A, 326, 950 (PEGASE)
Gallego, J., Zamorano, J., Aragon-Salamanca, A., & Rego, M. 1995, ApJ, 455, L1
Gilmore, G., & Howell, D., eds. 1998, ASP Conf. Ser. 142, The Stellar Initial Mass Function (San Francisco: ASP)
Glazebrook, K., et al. 2003, ApJ, 587, 55
Haarsma, D. B., Partridge, R. B., Windhorst, R. A., & Richards, E. A. 2000, ApJ, 544, 641
Hammer, F., et al. 1997, ApJ, 481, 49
Haywood, M. 2001, MNRAS, 325, 1365
Hogg, D. W. 2002, preprint (astro-ph/0105280v2)
Huang, J.-S., Cowie, L. L., Gardner, J. P., Hu, E. M., Songaila, A., & Wainscoat, R. J. 1997, ApJ, 476, 12
Huang, J.-S., Glazebrook, K., Cowie, L. L., & Tinney, C. 2003, ApJ, 584, 203
Hummer, D. G., & Storey, P. J. 1987, MNRAS, 224, 801
Kennicutt, R. C. 1983, ApJ, 272, 54
———. 1998, in ASP Conf. Ser. 142, The Stellar Initial Mass Function, ed. G. Gilmore & D. Howell (San Francisco: ASP), 1
Kennicutt, R. C., Tamblyn, P., & Congdon, C. E. 1994, ApJ, 435, 22
Kochanek, C. S., et al. 2001, ApJ, 560, 566
Kogut, A., et al. 2003, ApJ, submitted (astro-ph/0302213)
Kroupa, P. 2001, MNRAS, 322, 231
———. 2002, Science, 295, 82
Kroupa, P., Tout, C. A., & Gilmore, G. 1993, MNRAS, 262, 545
Kurucz, R. L. 1992, in IAU Symp. 149, The Stellar Populations of Galaxies, ed. B. Barbuy & A. Renzini (Dordrecht: Kluwer), 225
Lanzetta, K. M., Yahata, N., Pascarelle, S., Chen, H., & Fernández-Soto, A. 2002, ApJ, 570, 492
Lejeune, T., Cuisinier, F., & Buser, R. 1997, A&AS, 125, 229
Lilly, S. J., Le Fevre, O., Hammer, F., & Crampton, D. 1996, ApJ, 460, L1
Madau, P., Ferguson, H. C., Dickinson, M. E., Giavalisco, M., Steidel, C. C., & Fruchter, A. 1996, MNRAS, 283, 1388
Madau, P., Pozzetti, L., & Dickinson, M. 1998, ApJ, 498, 106
Maddox, S. J., Efstathiou, G., Sutherland, W. J., & Loveday, J. 1990, MNRAS, 243, 692
Madgwick, D. S., et al. 2002, MNRAS, 333, 133
Miller, G. E., & Scalo, J. M. 1979, ApJS, 41, 513
Milliard, B., Donas, J., Laget, M., Armand, C., & Vuillemin, A. 1992, A&A, 257, 24
Norberg, P., et al. 2002, MNRAS, 336, 907
Oke, J. B., & Gunn, J. E. 1983, ApJ, 266, 713
Pei, Y. C. 1992, ApJ, 395, 130
Rowan-Robinson, M., et al. 1997, MNRAS, 289, 490
Salpeter, E. E. 1955, ApJ, 121, 161
Saunders, W., Rowan-Robinson, M., Lawrence, A., Efstathiou, G., Kaiser, N., Ellis, R. S., & Frenk, C. S. 1990, MNRAS, 242, 318
Scalo, J. M. 1986, Fundam. Cosmic Phys., 11, 1
———. 1998, in ASP Conf. Ser. 142, The Stellar Initial Mass Function, ed. G. Gilmore & D. Howell (San Francisco: ASP), 201
Schechter, P. 1976, ApJ, 203, 297
Skrutskie, M. F., et al. 1997, in Impact of Large-Scale Near-IR Sky Surveys, ed. F. Garzóne (Dordrecht: Kluwer), 25
Spergel, D. N., et al. 2003, ApJ, submitted (astro-ph/0302209)
Spitzer, L. 1978, Physical Processes in the Interstellar Medium (New York: Wiley)
Steidel, C. C., Adelberger, K. L., Giavalisco, M., Dickinson, M., & Pettini, M. 1999, ApJ, 519, 1
Stoughton, C., et al. 2002, AJ, 123, 485
Strauss, M. A., et al. 2002, AJ, 124, 1810
Sullivan, M., Treyer, M. A., Ellis, R. S., Bridges, T. J., Milliard, B., & Donas, J. 2000, MNRAS, 312, 442
Tresse, L., & Maddox, S. J. 1998, ApJ, 495, 691
Treyer, M. A., Ellis, R. S., Milliard, B., Donas, J., & Bridges, T. J. 1998, MNRAS, 300, 303
Wolf, C., Meisenheimer, K., Rix, H.-W., Borch, A., Dye, S., & Kleinheinrich, M. 2003, A&A, 401, 73
Woosley, S. E., & Weaver, T. A. 1995, ApJS, 101, 181
Worthey, G. 1994, ApJS, 95, 107
Wright, E. L. 2001, ApJ, 556, L17
Wyse, R. F. G. 1997, ApJ, 490, L69
York, D. G., et al. 2000, AJ, 120, 1579